ADVANCED FUNCTIONAL MATERIALS
www.afm-journal.de

Fluorinated Polymer Yields High Organic Solar Cell Performance for a Wide Range of Morphologies

*John R. Tumbleston, Andrew C. Stuart, Eliot Gann, Wei You, and Harald Ade**

Device performance is recognized to be generally sensitive to morphology in bulk heterojunction solar cells. Through the use of quantitative morphological measurements, it is demonstrated that devices based on benzodithiophene and fluorinated benzotriazole moieties constitute an exception to this design rule and exhibit a range of morphologies that yield similar high performance. In particular, the fill factor (FF) remains above 65% even with factor of two changes in domain size and factor of two changes in relative domain purity. Devices with active layer thicknesses of 250 nm are employed, which are capable of increasing optical absorption to produce high photocurrent. The general insensitivity to both morphology and thickness is likely related to the measured low equilibrium miscibility of fullerene in the polymer of 3–4%. The materials and processes investigated therefore provide insights into functional material design that yield increased processing latitude and may be more amenable to roll-to-roll processing.

1. Introduction

The active layer morphology of organic solar cells is considered and shown to be in many cases a key factor that dictates power conversion efficiency (PCE) in bulk heterojunction (BHJ) photovoltaics.[1] Since the morphology can be manipulated with an appropriate choice of co-solvent,[2] addition of solvent additive,[3] or by thermal or solvent annealing after film deposition,[4] a wide parameter space exists for active layer formation. This has led to a plethora of observed morphologies, characterized with techniques based on scanning probes,[5] X-rays,[6,7] electrons,[8] and neutrons.[9] For most BHJ systems, optimized performance is achieved by varying processing conditions with a corresponding morphology distinctly different from those for lower performing devices. This has led to the assumption and paradigm that specific morphological characteristics must be obtained in order to achieve high performance, with a narrow window for deviation. Specifically, pure domains with lateral in-plane dimensions on the order of the exciton diffusion length of ~10 nm[10] are generally considered to be ideal and necessary. This paradigm is commonly supported by morphological probes that only provide qualitative information. While helpful, qualitative measurements may exaggerate differences in morphology between devices or conversely show that differences in morphological parameters, such as domain purity, are minor when they are actually substantial.

In this work, we demonstrate that devices based on a high performance polymer defy the typically asserted sensitivity of device performance to morphology. When blended with phenyl-C61-butyric acid methyl ester (PCBM), a weak-donor strong-acceptor polymer that combines benzodithiophene (BnDT) and fluorinated benzotriazole (FTAZ) units, shows a remarkable indifference to BHJ morphology, i.e., domain size and purity, which is controlled by varying processing conditions. PBnDT-FTAZ belongs to the growing number of polymers achieving PCE of 7%.[11–14] High performance is due in part to fluorination of the polymer backbone, a polymer design scheme used to boost performance for other BHJ blends.[13–16] We show that high performance can be achieved with a remarkable range of in-plane domain size distributions and domain purities for PBnDT-FTAZ:PCBM. Specifically, varying the domain spacing and relative domain purity by over a factor of two does not reduce the fill factor (FF) below 65%, while increasing the in-plane domain spacing from ~50 nm by more than a factor of two to 130 nm still yields high short-circuit current (J_{SC}). This work also reveals morphological characteristics of this high performance system that includes large domain spacing and low polymer crystallinity, which contrasts with prototypical systems like P3HT:PCBM.[17] Ultimately, this work highlights that morphological variability within the range we measure is not detrimental to device performance for this system. We find an extremely low equilibrium miscibility of PCBM in PBnDT-FTAZ as observed in solvent annealed samples, which helps explain our observations by providing insight into the molecular interactions between these two materials and is likely influenced by the backbone fluorination.

2. Results and Discussion

Figure 1 shows the chemical structure of PBnDT-FTAZ along with representative current density vs. voltage (*J–V*) curves under 1 Sun illumination when casting from three different

Dr. J. R. Tumbleston, E. Gann, Prof. H. Ade
Department of Physics
North Carolina State University
Raleigh, NC, 27695, USA
E-mail: hwade@ncsu.edu
Dr. A. C. Stuart, Prof. W. You
Department of Chemistry
University of North Carolina at Chapel Hill
Chapel Hill, NC, 27599, USA

DOI: 10.1002/adfm.201300093

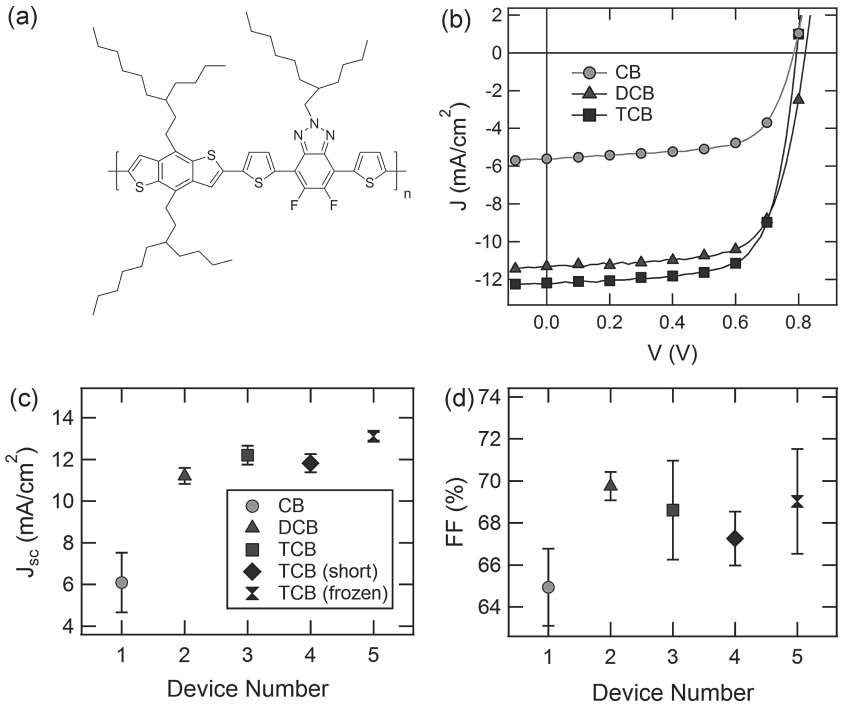

Figure 1. a) Chemical structure of PBnDT-FTAZ. b) Representative current density vs. voltage under 1 Sun illumination for PBnDT-FTAZ:PCBM devices processed from CB, DCB, and TCB. c) J_{sc} and d) FF for these devices along with two other devices processed from TCB (number 4 and 5) that experience shorter solvent annealing times compared to the normal TCB device (number 3). While changes are noted in the J_{sc} with respect to processing condition, the FF remains at least 65% for all samples indicating minimal voltage-dependent recombination losses.

solvents, chlorobenzene (CB), 1,2-dichlorobenzene (DCB), and 1,2,4-trichlorobenzene (TCB). In terms of J_{sc}, a general improvement is noted as the boiling point of the solvent is increased from T_b = 131 °C (CB) to T_b = 181 °C (DCB) to T_b = 214 °C (TCB). Less variation is observed in the open-circuit voltage (V_{oc}) and FF, which remain nearly fixed at 0.77 V and 66%, respectively. The high FF above 65% is a noteworthy trait of this system. Relatively thick (~250 nm) active layers are used for all devices in this work to enhance optical absorption above what is possible with typical active layer thicknesses of ~100 nm. Use of thicker active layers has the added benefit of being more amenable to roll-to-roll processing since films of this thickness have been shown to be optimal for roll-to-roll slot-die coated solar modules.[18] Furthermore, after solution casting, films are merely allowed to dry in a closed petri dish overnight prior to electrode deposition and are not thermally treated (see Experimental section for fabrication details). Even though we do use thermally evaporated electrodes not compatible with roll-to-roll processing (e.g., calcium and aluminium), we believe the processing latitude and active layer thickness afforded by PBnDT-FTAZ:PCBM makes it a strong candidate or at least a model system for high performance roll-to-roll solar modules.

Since changes in performance with solvent are primarily noted in J_{sc}, two other preparation conditions are added in order to broaden the parameter space of processing conditions. Reducing the drying time for TCB cast films was achieved using a larger petri dish for solvent drying (TCB (short)) and by vacuum drying at 30 mmHg below atmosphere for 10 min immediately after spin-coating (TCB (frozen)). Performance parameters are shown in Figure 1b,c and listed in **Table 1** for all processing conditions of this study. Interestingly, all processing conditions, except for CB processing, show good performance with PCE above 5.8%, or within 17% of the highest values demonstrated for this system in this or in previous work (PCE = 7.0%).[12] Individual performance parameters are also within 15% of the highest values, especially the FF, which remains at or above the excellent 65% level for all devices. The most significant performance reduction is for devices processed from CB where the J_{sc} is reduced (Figure 1b) by over a factor of two from 13.1 to 6 mA/cm^2. It should be noted that there are insignificant changes in absorption from UV-vis measurements (see Supporting Information Figure S1), so this drop in J_{sc} is asserted to be due to changes in internal quantum efficiency, not absorption efficiency.

Given the similarity in device performance for the four devices with PCE ≥ 5.8%, it is expected that the morphological and structural traits of the active layer are similar for these blend films whereas the properties of the CB-cast devices are very different. In particular, polymer crystallinity, orientation, and size have been shown to correlate with device performance for many systems.[19] Crystallinity and d-spacing[20] of π–π stacked polymer chains have received special attention due to the relatively efficient charge transport characteristics associated with this stacking direction. Herein, structural properties were measured with grazing incidence wide angle X-ray scattering (GIWAXS) of blend films at beamline 7.3.3 of the Advanced Light Source.[21] Films were prepared on PEDOT:PSS-coated silicon substrates following the same preparation conditions as used for devices (see Experimental section for details). **Figure 2**a shows out-of-plane and in-plane 20° sector averages that reveal the presence of polymer lamellar (100) and π–π stacking (010) reflections along with the customary signature from PCBM near q = 1.4 nm^{-1}. Overall, polymer crystallinity is observed

Table 1. Average device performance with different processing conditions for PBnDT-FTAZ:PCBM devices.

Device Number	Processing Condition	Thickness [nm]	V_{oc} [V]	J_{sc} [mA/cm^2]	FF [%]	PCE [%]
1	CB	270 ± 5	0.79 ± 0.01	6 ± 1	65 ± 2	3.1 ± 0.8
2	DCB	245 ± 5	0.82 ± 0.01	11.2 ± 0.4	70 ± 1	6.4 ± 0.3
3	TCB	260 ± 5	0.79 ± 0.01	12.2 ± 0.4	69 ± 2	6.6 ± 0.3
4	TCB (short)	250 ± 5	0.74 ± 0.01	11.8 ± 0.4	67 ± 1	5.8 ± 0.3
5	TCB (frozen)	242 ± 5	0.77 ± 0.01	13.1 ± 0.2	69 ± 2	7.0 ± 0.4

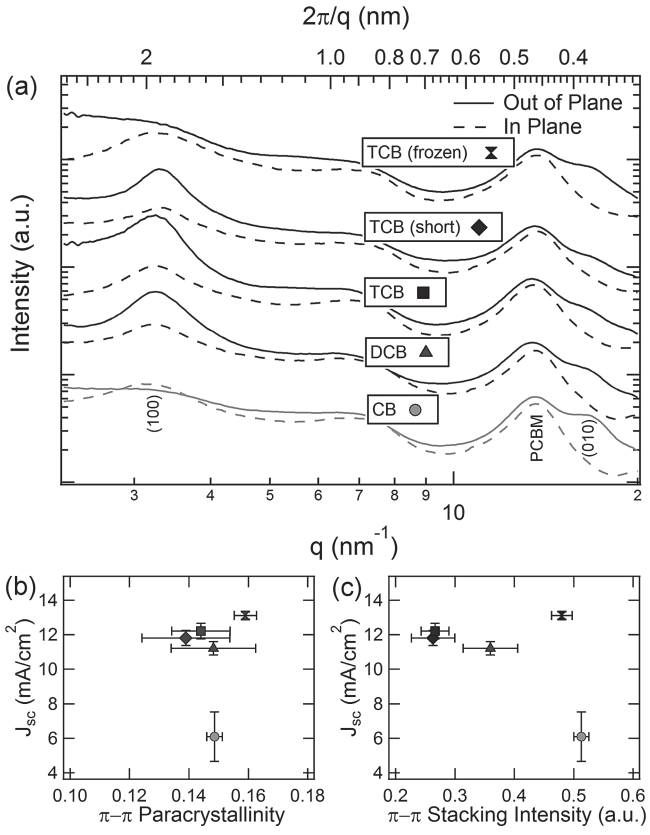

Figure 2. a) GIWAXS out-of-plane and in-plane 20° sector averages of the five blend films of this study where traces have been scaled vertically for ease of view (log y-axis). b) J_{sc} as function of out-of-plane π–π stacked paracrystallinity factor and c) scattering peak intensity. There is no significant correlation with device performance. This is best exemplified by comparing CB to TCB (frozen) data which shows similar scattering even though PCE is 3.1% and 7.0%, respectively.

to be relatively low, or rather the paracrystallinity[6] is high compared to other semicrystalline blends due to the complete absence of any higher order reflections. Hence, crystallinity and long range order will likely play a minor role in determining device performance. The differences that were observed did not correlate to performance.

Specifically, neither the lamellar (1.9 nm) nor π–π (0.38 nm) d-spacings significantly change with processing. Likewise, the π–π out-of-plane crystallite size as determined from Scherrer analysis remains essentially fixed at 2.5–3 nm (see Supporting Information Figure S2 and Table S1). Given the d-spacing of π–π crystal planes, this crystal size corresponds to crystallites of ~8 polymer chains. However, it is not likely that the peak broadening originates from crystals with well-defined grain boundaries. Rather, peak broadening arises due to cumulative lattice disorder that can be quantified via a paracrystallinity factor, g.[22] For all samples, g ~ 0.14 for π–π stacking (Figure 2b), which is comparable to the value of 0.12 for SiO_2 glass and is much higher when compared to semicrystalline polymers where g < 0.08.

The most noted variation in the GIWAXS measurement with processing occurs for the intensity of the π–π reflections, which is a measure of the relative degree of ordering and/or relative orientation with respect to the electrodes. These intensities are determined by normalizing the π–π stacking intensities to the diffuse PCBM peak intensities. As shown in Figure 2c, even though there are significant differences in this structural metric, there is no correlation with J_{sc}. The highest intensity occurs for the CB and TCB (frozen) films which have the lowest and highest J_{sc}, respectively. As the solvent annealing time increases either by using a solvent with higher boiling point or by allowing for longer drying time, the π–π out-of-plane intensity is reduced, while the lamellar intensity increases. This indicates a reorientation of polymer crystallites during solvent annealing to an orientation that is comparatively more "edge-on" with the polymer side chains perpendicular to the substrate.

The metrics from crystallinity analysis indicate that the overall crystallinity is relatively low and that crystallite orientation can take on a range of conformations and still yield high J_{sc}. Complimentary to GIWAXS, resonant soft x-ray scattering (R-SoXS) is sensitive to compositional differences within blend films and probes the compositional domain size distribution from a few nanometers to microns.[23] This technique is sensitive to both crystalline and amorphous regions within the films and is therefore uniquely sensitive to the compositional morphology in these highly amorphous films. R-SoXS was conducted at beamline 11.0.1.2 of the Advanced Light Source[24] and involves illuminating a thin film in a transmission geometry (measuring in-plane structure only) and collecting the scattered X-rays. Azimuthally integrating the 2D scattering intensity yields the scattering profiles in **Figure 3**a. Since the incident photon energy can be selected, R-SoXS takes advantage of the materials specific complex indices of refraction ($\tilde{n} = 1–\delta + i\beta$) near the carbon 1s absorption edge for each material. The real dispersive part, δ, and the imaginary absorptive part, β, for PBnDT-FTAZ and PCBM (Figure 3b) are unique fingerprints of each material and provides scattering contrast that is proportional to $\Delta n^2 = (\Delta\delta)^2 + (\Delta\beta)^2$.

For energies well below the absorption edge of both materials (e.g. 270 eV), the material contrast between polymer and fullerene is low, while each individual material has high contrast with vacuum (Figure 3c). Therfore, scattering will be dominated by mass-thickness contrast if there is significant surface roughness or thickness variations. Conversly, for energies near the absorption edges of each material, optical contrast between PBnDT-FTAZ and PCBM is high (Figure 3c). The tunability of the contrast is evident in differences in scattering profiles for the TCB (short) devices in Figure 3a. Overall, similar scattering patterns are observed with the primary difference being the scattering intensity. Differences in shape are observed only for 288.2 eV due to a fluorescent background at high q, and for 270 eV where a low q-feature is present due to mass-thickness differences that are unrelated to compositional variations. The 284.1 eV data is completely dominated by compositional differences (details provided below). The broad scattering peak observed represents the distribution of domain spacings between like domains in the bulk of the thin film.[25] The peak in the scattering profile occurs at q ~ 0.09 nm^{-1}, which corresponds to a dominant domain spacing of $2\pi/q = 70$ nm.

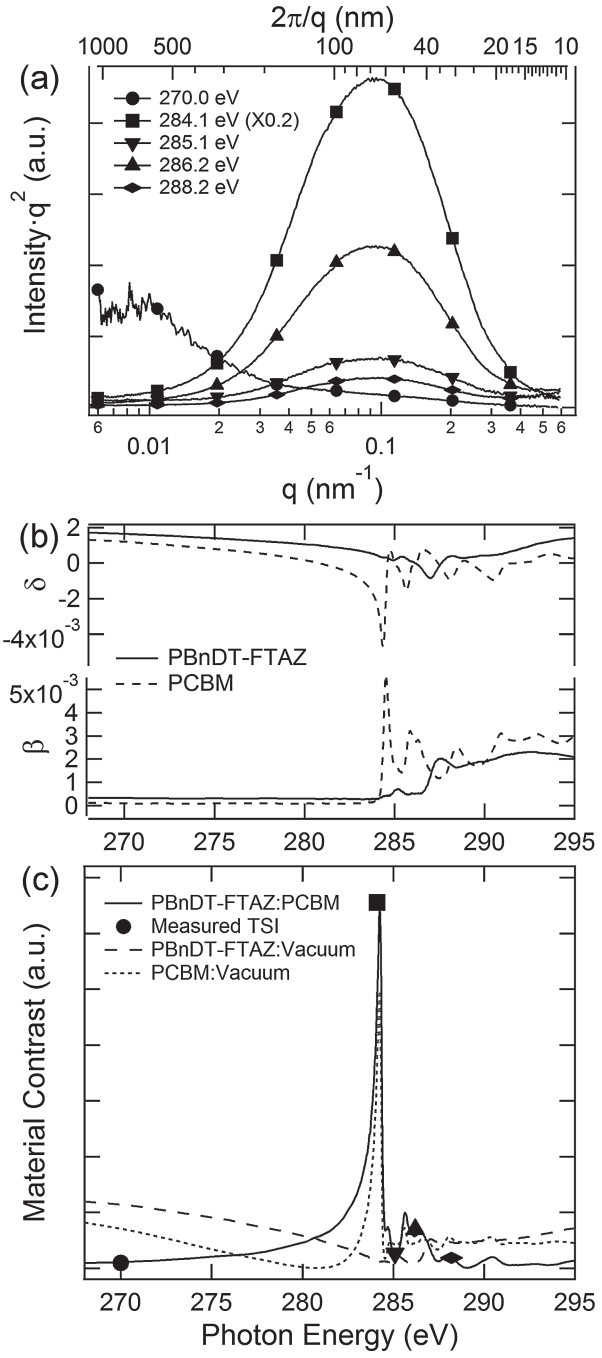

Figure 3. a) Azimuthally integrated R-SoXS of PBnDT-FTAZ:PCBM blend film processed from TCB (short) for different incident photon energies (linear y-axis). Optical contrast between PBnDT-FTAZ and PCBM dominates the scattering (270.0 eV has an additional low-q feature), which results in similar scattering profiles with a broad peak that represents the distribution of domain spacings. Data for 284.1 eV photon energy has been scaled by 0.2. b) Real and imaginary parts of the indices of refraction ($\tilde{n} = 1-\delta + i\beta$) for PBnDT-FTAZ and PCBM near the carbon 1s absorption edge, where δ is the real, dispersive part and β is the imaginary, absorptive part, respectively. c) Energy dependent material contrast for polymer:fullerene, polymer:vacuum, and fullerene:vacuum that is proportional to $\Delta n^2 = (\Delta\delta)^2 + (\Delta\beta)^2$. Contrast has been multiplied by a Beer-Lambert correction factor to account for absorption. Integrations of the scattering profiles in (a) correspond to the TSI and follow the material contrast between PBnDT-FTAZ and PCBM.

To confirm that scattering originates from optical contrast between polymer-rich and fullerene-rich domains, the scattering profiles of Figure 3a are integrated to yield the total scattering intensity (TSI),[25] also known as Porod's invariant.[26] These TSI values track the materials contrast between PBnDT-FTAZ and PCBM and not either of the two vacuum contrast functions (Figure 3c). It should be noted that the scattering contrast is corrected for absorption within the film by multiplying by the Beer-Lambert factor, $\exp(-4\pi d\langle\beta\rangle/\lambda)$, where λ is the incident photon wavelength, d, is the film thickness, and $\langle\beta\rangle$ is the compositionally averaged imaginary part of the index of refraction. Correcting for absorption provides the correct comparison of the energy dependence of the TSI to the contrast function. Finally, for energies below the lowest energy absorption peaks at 285.1 and 284.4 eV for polymer and fullerene, respectively, there is less absorption and thus less susceptibility to beam damage. Furthermore, since no core-hole is created at 284.1 eV, there is also minimal X-ray fluorescence as observed as a change in slope near q = 0.3 nm^{-1} in Figure 3a. This background is most pronounced for 288.2 eV where X-ray absorption is greatest.

Figure 4a shows the R-SoXS scattering curves for PBnDT-FTAZ:PCBM blends processed with five different preparation conditions. A photon energy just below the absorption edge (284.1 eV) is used to provide high material optical contrast due to δ differences between polymer and fullerene while also avoiding beam damage and X-ray fluorescence. The peak locations and scattering intensities are highly sensitive to processing conditions. The J_{sc} and FF are plotted as functions of dominant domain spacing in Figure 4b,c where the range in size varies by over 2.5 times from 50 nm for TCB (frozen) to 135 nm for DCB processed devices. Remarkably, high performance is achieved regardless of this variation in morphology. All blends are 1:2 w/w of polymer to PCBM, so assuming the same volume ratio for polymer-rich and fullerene-rich domains in a two phase system, the largest spacing corresponds to dominant domain sizes of 135 nm·33% = 45 nm and 135 nm·66% = 90 nm for polymer and fullerene domains, respectively, for the DCB processed devices. While the J_{sc} does show some relation with domain spacing where the larger domains have lower J_{sc} and the smaller domains have higher J_{sc}, the relative insensitivity to domain size is unexpected. For example, the DCB processed devices have a dominant domain spacing that is over 2.5 times larger than the TCB (frozen) devices yet the J_{sc} is only reduced by 15%. The large domain size of the DCB devices is also slightly greater than for those processed from CB indicating that the J_{sc} reduction for CB devices is not due to the large measured domain size. Therefore, from size measurements alone using R-SoXS or a surface sensitive measurement such as atomic force microscopy (Supporting Information Figure S3), it is difficult to understand the morphological drivers of performance.

Also computed from the scattering curves are the relative domain purities averaged over the length scales probed by R-SoXS (Supporting Information Figure S4 for integration comparisons). Within a two phase model, domain purity is proportional to the square root of the TSI[25] where TCB devices exhibit the highest TSI and thus have the highest relative domain purity. For more mixed domains, the total scattering intensity

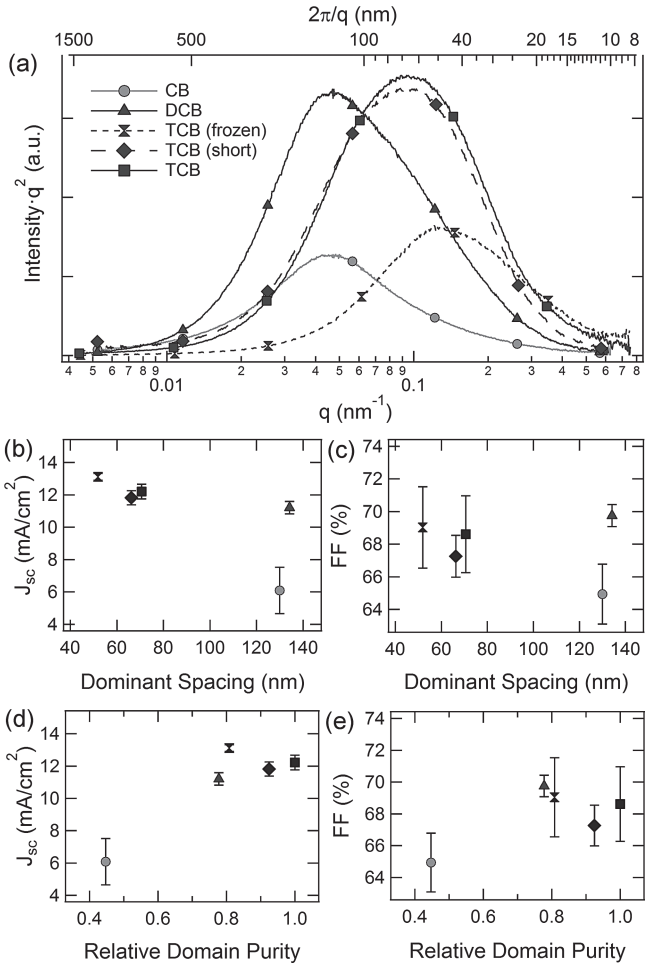

Figure 4. a) R-SoXS scattering curves for 284.1 eV photon energy for different preparation conditions of PBnDT-FTAZ:PCBM blends (linear y-axis). The peaks correspond to dominant domain spacings and are plotted against b) J_{sc} and c) FF. The relative domain purities as determined from the total scattering intensities of the scattering curves are also compared to d) J_{sc} and e) FF. Relative domain purity represents the difference in composition between polymer-rich and fullerene-rich domains for each sample where a value of zero would correspond to domains that are fully mixed.

is lower than for purer domains due to reduced optical contrast. Values of relative domain purity are shown in Figure 4d,e plotted against J_{sc} and FF. As with domain spacing, large variations in purity are observed. The low J_{sc} of the CB processed devices is likely due to the low domain purity corresponding to highly mixed domains. Even though the domain size is nearly the same as for the DCB processed devices, the compositional differences between polymer-rich and fullerene-rich domains in each sample are 0.78/0.45 = 1.7 times greater for DCB compared to CB-cast devices. The 0.45 composition difference between domains for the CB devices corresponds to domains with 73% majority and 28% minority component assuming domains with equal minority content. Thus purity, not size, is a likely explanation for the difference in J_{sc} between CB and DCB devices. Once a certain threshold is reached in domain purity, it is not observed to be a critical parameter affecting J_{sc}. Importantly, Figure 4 reveals that domain mixing is not detrimental to device performance within a certain range since TCB (frozen) devices have a relative domain purity of 0.8 and also the highest J_{sc} and PCE. Even less sensitive to purity differences is the FF where the full range of relative purities that varies by 2.3 times always yields exceptionally high FF at or above 65%. The noted compositional differences are likely related to film drying time since the purities track the boiling point of the three solvents with CB processed films representing a morphology quenched in a disordered/mixed state. This is supported within the set of samples processed with TCB where purity increases from TCB (frozen) to TCB (short) to TCB. Finally, vertical phase separation and wetting layers[27] cannot be ruled out from influencing performance. However, significant differences in vertical composition profiles between the devices would likely add to the appeal of this system as this would be yet another morphological parameter that does not strongly drive performance. The original publication on PBnDT-FTAZ also included vertical composition analysis that did not show any major vertical material segregation for TCB processed devices.[12]

While J_{sc} is noted to drop for very impure domains in the case of the CB devices, slightly mixed domains do not strongly reduce photocurrent as observed for those processed as DCB and TCB (frozen). It has been argued that a certain level of mixing is advantageous for devices to retain percolation pathways to the electrodes in some systems,[28] and is likely more important for larger domains.[29] Unfortunately, the absolute domain purities are not known from the relative measurements above. However, an absolute upper limit is obtained for purity by measuring the molecular miscibility of PCBM in PBnDT-FTAZ at equilibrium. Molecular miscibility reflects the propensity for polymer and fullerene to mix in the amorphous portions of the polymer, which is likely a universal occurrence in OPV devices.[25,30,31] In order to measure miscibility, samples are prepared by solvent annealing blend films in a closed container saturated with TCB solvent vapor. After four days of solvent annealing, the resulting morphology (**Figure 5**a,b) consists of PCBM crystals tens of microns in size surrounded by polymer matrix that has reached local equilibrium with the crystals (Supporting Information Figure S5). This equilibrium composition and hence miscibility is measured with scanning transmission X-ray microscopy (STXM) at beamline 5.3.2.2 of the Advanced Light Source[32] following previously established methods.[33] Fitting the measured reference spectra of pure polymer and fullerene to an absorption spectrum acquired of the polymer-rich matrix between PCBM crystals yields 3.7 ± 0.2% residual PCBM in PBnDT-FTAZ. An identical final composition was obtained for samples annealed in CB vapour (Supporting Information Figure S6) showing that the same equilibrium composition is reached regardless of the annealing solvent. This miscibility value therefore sets an absolute upper limit of the domain purity in the TCB processed sample that has the highest TSI to be ~96%. It should be noted that crystalline PCBM has been recently shown to induce greater purification than amorphous PCBM agglomerates when thermally annealing mixtures of semicrystalline poly(3-hexylthiophene) and PCBM.[34] Both the imaging (Figure 5a,b) and GIWAXS of the equilibrated films (Supporting Information Figure S7) support the presence of

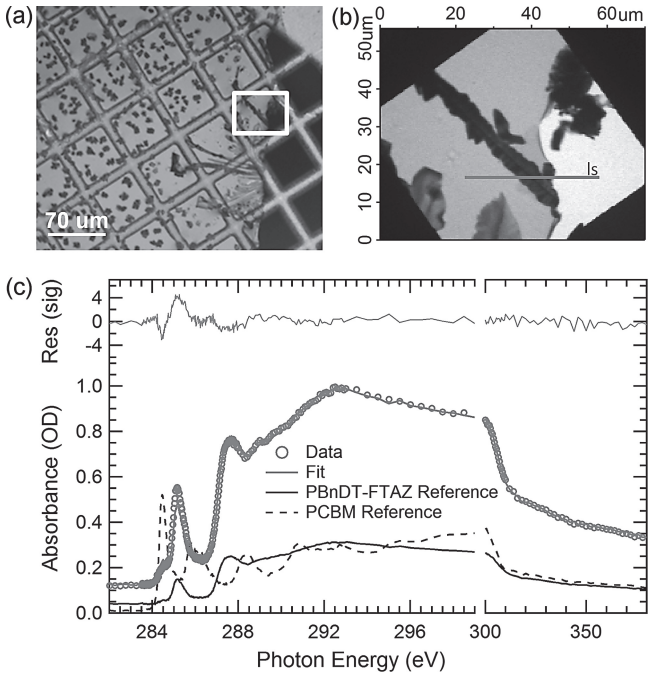

Figure 5. a) Reflective visible light microscope and b) STXM images of four day TCB solvent annealed blend films with equilibrated phase separation (dark spots are PCBM crystals). c) Absorption spectrum between PCBM crystals (derived from line-scan spectra along line in (b) marked "ls") and corresponding fit using the measured reference spectra of pure PBnDT-FTAZ and PCBM. Miscibility of PCBM in the polymer matrix is 3-4% regardless of annealing solvent.

PCBM crystals after prolonged solvent annealing which would lead to an overestimation of the upper purity limit in devices since they do not have PCBM crystals. Even so, compared to the miscibility of fullerene in other OPV polymers where PCBM crystallization is induced,[25,31] for which 15–50% PCBM in the amorphous region of the polymer has been observed, the miscibility in PBnDT-FTAZ is exceedingly low.

Overall, the structural and morphological data indicate that device performance of PBnDT-FTAZ:PCBM is not highly sensitive to domain spacing or domain purity within a certain range. In particular the FF is always above 65%, even though the domain size and average domain purity each change by a factor of two. It should be emphasized that FF ≥ 65% indicates that recombination losses that depend on the applied voltage are not significant in these devices. These include bimolecular recombination,[35] a voltage-dependent dissociation of charge transfer states at donor/acceptor interfaces,[36] and certain types of charge trapping.[37] This level of insensitivity to domain purity in this system is surprising considering that Monte Carlo modelling support the general importance of purity[29,38] along with experimental measurements in other systems.[15] Not only is this unexpected from a morphological standpoint, but also from the perspective of active layer thickness since ~250 nm active layers are used in all devices. Likewise, FF = 54% was previously achieved for active layer thicknesses of 1000 nm,[12] which indicates exceptionally low voltage-dependent recombination losses (e.g., bimolecular recombination) for this thickness. Therefore, there must be an interaction between polymer and fullerene that successfully stifles recombination losses. This hypothesis is also supported by measurements of space charge limited hole mobilities in blend films with values of ~10^{-3} cm^2/Vs,[12] which are typical of other BHJ blends and thus cannot explain the high FF.

As a first or correlated explanation, the measurement of less than 4% PCBM miscibility in PBnDT-FTAZ (Figure 5) is exceedingly low compared to other primarily amorphous polymers which typically exhibit at least 15% fullerene miscibility.[25,31,34] This exceptionally low miscibility indicates that energetic barriers exist between PBnDT-FTAZ and PCBM molecules which limit their molecular mixing. In other words, these two materials prefer not to be in close proximity with each other and will phase separate if given the opportunity in the presence of solvent. This molecular level repulsion could be amenable to charge transport where holes remain confined to the polymer and electrons to PCBM despite relatively thick active layers, only moderate hole mobilities, and a range morphological characteristics. Furthermore, this preferential repulsive interaction is likely influenced by the presence of fluorine on the polymer backbone. Consequently, larger domains have been noted in blends comprised of polymers with fluorinated backbones compared with their nonfluorinated counterparts[14,15,39] in part due to an argued fluorophobicity between polymer and fullerene.[14] This is consistent with the morphology results and the very low miscibility of polymer and fullerene measured here.

While potentially stifling recombination, the impact of the low miscibility on driving morphological development is important when choosing processing protocols that optimize performance. As evidenced from the TCB (frozen) device with the highest J_{sc}, which has the smallest domains and some level of advantageous mixing, it is important to find processing conditions that allow for domains to be relatively small while also having optimal purity. Processing techniques are required that counteract the propensity of low miscibility blends to phase separate too much while also not being quenched in a highly mixed state.

3. Conclusion

In conclusion, the low measured equilibrium miscibility of PCBM in PBnDT-FTAZ is an important aspect of this polymer that drives morphological development in different solvents and likely helps reduce recombination losses. High performance is achieved for a range of BHJ morphologies. Specifically, FF values of at least 65% are achieved even when the in-plane domain spacing and relative domain purity change by factors of two. Even though there is a general insensitivity of device performance to morphology, if the domains are too impure J_{sc} is impacted and is significantly reduced as observed in the blend processed from CB. However, this loss process is not strongly electric field dependent as the FF is not significantly reduced. More broadly, PBnDT-FTAZ is a polymer that provides a large working window for eventual high volume processing where precise morphological control may be difficult or not economically viable. The observed unusual performance is highly likely related to the material used, i.e., the substitution of fluorine on

the backbone of the polymer, altering the interaction with the fullerene in a beneficial way. More detailed studies of molecular interactions and possibly molecular ordering at the bulk heterojunction interface[40] due to fluorine substitution are required to fully elucidate this system.

4. Experimental Section

Device Fabrication and Characterization: Poly(4,8-bis(3-butylnonyl) benzo[1,2-b:4,5-b′]dithiophen-2-yl)thiophen-2-yl)-2-(2-butyloctyl)-5,6-difluoro-7-(thiophen-2-yl)-2H-benzo[d][1,2,3]triazole) (PBnDT-FTAZ) was used from the same batch as for previous work with $M_n = 42.2$ kg/mol and PDI = 2.36.[12] Glass substrates coated with patterned indium-doped tin oxide (ITO) were purchased from Thin Film Devices, Inc. The 150 nm sputtered ITO pattern had a resistivity of 15Ω/□. Prior to use, the substrates were ultrasonicated for 20 min in 2-propanol. The substrates were dried under a stream of nitrogen and subjected to the treatment of UV-Ozone for 30 min. A filtered dispersion of PEDOT:PSS in water (Baytron PH500) was then spun cast onto clean ITO substrates at 4000 rpm for 60 s and then baked at 140 °C for 10 min to give a thin film with a thickness of 40 nm. Blends of PBnDT-FTAZ:PCBM (1:2 w/w, 12 mg/mL for polymer) were dissolved in solvent with heating at 120–140 °C for 6 h. Blend films were spincast on PEDOT:PSS at an RPM between 400 and 550 for 60 s with no thermal post-processing. The devices were finished for measurement after thermal deposition of a 30 nm film of calcium and a 70 nm aluminum film as the cathode at a base pressure of 1×10^{-6} mbar. There are 8 devices per substrate, with an active area of 12 mm^2 per device. Device characterization was carried out under AM 1.5G irradiation with the intensity of 100 mW/cm^2 (Oriel 91160, 300 W) calibrated by a NREL certified standard silicon cell. Current density versus voltage (*J*–*V*) curves were recorded with a Keithley 2400 digital source meter. All fabrication steps after adding the PEDOT:PSS layer onto ITO substrate, and characterizations were performed in gloveboxes under nitrogen atmosphere. The thicknesses of films were recorded by a profilometer (Alpha-Step 200, Tencor Instruments). Samples for X-ray characterization were prepared on PEDOT:PSS-coated Si substrates and processed in an identical manner as those used in devices. To double-check that no changes occurred due to substrate differences or unintentional processing variations compared to those used in devices, R-SoXS measurements were conducted on films floated from actual devices. No significant differences were observed (see Supporting Information Figure S8).

X-Ray Characterization: R-SoXS characterization was conducted at Beamline 11.0.1.2 of the Advanced Light Source (ALS)[24] in the soft X-ray energy regime (~280 eV). A section of film from the PEDOT:PSS-coated Si substrates was floated onto 1.5 mm × 1.5 mm silicon nitride windows. The 1D averaged intensity is multiplied by q^2, which then corresponds to an azimuthal integration of the 2D data. This more directly reflects the fractional distribution of domain spacing than the traditional 1D I(q) function as $I(q)\cdot q^2$ resembles the power spectral density of the 2D data.[25] GIWAXS was carried out at Beamline 7.3.3. of the ALS[21] using a Dectris Pilatus 1M photon counting detector. Blend films were measured at an incident angle of ~0.14°, above the critical angle so the X-ray beam penetrated to the substrate. The photon energy used for GIWAXS was 10 keV. Air scatter which provides a background signal was reduced using helium gas. Data was not corrected for the missing wedge in the out of plane direction.[6] STXM was conducted at Beamline 5.3.2.2 of the ALS.[32] Films cast on PEDOT:PSS-coated Si substrates were floated onto TEM grids. During measurement, the chamber was filled with 1/3 ATM He. The imaginary part of the index of refraction of pure materials is determined from STXM measurements and is then used to calculate the real part via a Kramers-Kronig transformation. Mass densities of 1.1 and 1.3 g/cm^3 for polymer and fullerene are assumed to calculate the complex indices of refraction.

Supporting Information

Supporting Information is available from the Wiley Online Library or from the author.

Acknowledgements

X-ray characterization and analysis by J.T., E.G., and H.A. were supported by DOE, OS, BES, MSE (DE-FG02-98ER45737). Data were acquired at Beamlines 5.3.2.2, 7.3.3, and 11.0.1.2 of the ALS, which is supported by DOE (DE-AC02-05CH1123). Thanks are given to David Kilcoyne at beamline 5.3.2.2, Alexander Hexemer, Eric Schaible, and Steven Alvarez at beamline 7.3.3, and Cheng Wang and Anthony Young at beamline 11.0.1.2 for assistance with data acquisition. Brian A. Collins is also acknowledged for many helpful discussions along with Terry McAfee and Subhrangsu Mukherjee for assistance with STXM data acquisition. Wentao Li assisted with polymer synthesis. A.C.S. and W.Y. were supported by Office of Naval Research (N000141110235) and an NSF CAREER Award (DMR-0954280). W.Y. is a Camille Dreyfus Teacher-Scholar.

Received: September 17, 2012
Revised: November 21, 2012
Published online: February 15, 2013

[1] a) L.-M. Chen, Z. Hong, G. Li, Y. Yang, *Adv. Mater.* **2009**, *21*, 1434; b) M. A. Brady, G. M. Su, M. L. Chabinyc, *Soft Matter* **2011**, *7*, 11065; c) R. Giridharagopal, D. S. Ginger, *J. Phys. Chem. Lett.* **2010**, *1*, 1160; d) M. A. Ruderer, P. Muller-Buschbaum, *Soft Matter* **2011**, *7*, 5482.

[2] S. H. Park, A. Roy, S. Beaupre, S. Cho, N. Coates, J. S. Moon, D. Moses, M. Leclerc, K. Lee, A. J. Heeger, *Nat. Photonics* **2009**, *3*, 297.

[3] J. K. Lee, W. L. Ma, C. J. Brabec, J. Yuen, J. S. Moon, J. Y. Kim, K. Lee, G. C. Bazan, A. J. Heeger, *J. Am. Chem. Soc.* **2008**, *130*, 3619.

[4] a) G. Li, V. Shrotriya, J. S. Huang, Y. Yao, T. Moriarty, K. Emery, Y. Yang, *Nat. Mater.* **2005**, *4*, 864; b) W. L. Ma, C. Y. Yang, X. Gong, K. Lee, A. J. Heeger, *Adv. Funct. Mater.* **2005**, *15*, 1617.

[5] C. Groves, O. G. Reid, D. S. Ginger, *Acc. Chem. Res.* **2010**, *43*, 612.

[6] J. Rivnay, S. C. B. Mannsfeld, C. E. Miller, A. Salleo, M. F. Toney, *Chem. Rev.* **2012**, *112*, 5488.

[7] C. R. McNeill, H. Ade, *J. Mater. Chem. C* **2013**, *1*, 187.

[8] a) A. A. Herzing, L. J. Richter, I. M. Anderson, *J. Phys. Chem. C* **2010**, *114*, 17501; b) M. Pfannmöller, H. Flügge, G. Benner, I. Wacker, C. Sommer, M. Hanselmann, S. Schmale, H. Schmidt, F. A. Hamprecht, T. Rabe, W. Kowalsky, R. R. Schröder, *Nano Lett.* **2011**, *11*, 3099.

[9] a) W. Yin, M. Dadmun, *ACS Nano* **2011**, *5*, 4756; b) J. W. Kiel, A. P. R. Eberle, M. E. Mackay, *Phys. Rev. Lett.* **2010**, *105*, 168701.

[10] P. E. Shaw, A. Ruseckas, I. D. W. Samuel, *Adv. Mater.* **2008**, *20*, 3516.

[11] a) Y.-X. Xu, C.-C. Chueh, H.-L. Yip, F.-Z. Ding, Y.-X. Li, C.-Z. Li, X. Li, W.-C. Chen, A. K. Y. Jen, *Adv. Mater.* **2012**, *24*, 6356; b) Y. Liang, Z. Xu, J. Xia, S.-T. Tsai, Y. Wu, G. Li, C. Ray, L. Yu, *Adv. Mater.* **2010**, *22*, E135; c) T.-Y. Chu, J. Lu, S. Beaupré, Y. Zhang, J.-R. Pouliot, S. Wakim, J. Zhou, M. Leclerc, Z. Li, J. Ding, Y. Tao, *J. Am. Chem. Soc.* **2011**, *133*, 4250; d) C. M. Amb, S. Chen, K. R. Graham, J. Subbiah, C. E. Small, F. So, J. R. Reynolds, *J. Am. Chem. Soc.* **2011**, *133*, 10062; e) X. Guo, M. Zhang, J. Tan, S. Zhang, L. Huo, W. Hu, Y. Li, J. Hou, *Adv. Mater.* **2012**, *24*, 6536; f) L. Huo, S. Zhang, X. Guo, F. Xu, Y. Li, J. Hou, *Angew. Chem. Int. Ed.* **2011**, *50*, 9697; g) Y. Huang, X. Guo, F. Liu, L. Huo, Y. Chen, T. P. Russell, C. C. Han, Y. Li, J. Hou, *Adv. Mater.* **2012**, *24*, 3383; h) T. Yang, M. Wang, C. Duan, X. Hu, L. Huang, J. Peng, F. Huang, X. Gong, *Energy Environ. Sci.* **2012**, *5*, 8208; i) M.-S. Su, C.-Y. Kuo, M.-C. Yuan, U. S. Jeng, C.-J. Su, K.-H. Wei, *Adv. Mater.* **2011**, *23*, 3315.

[12] S. C. Price, A. C. Stuart, L. Yang, H. Zhou, W. You, *J. Am. Chem. Soc.* **2011**, *133*, 4625.
[13] a) H. Zhou, L. Yang, A. C. Stuart, S. C. Price, S. Liu, W. You, *Angew. Chem. Int. Ed.* **2011**, *50*, 2995; b) H.-Y. Chen, J. Hou, S. Zhang, Y. Liang, G. Yang, Y. Yang, L. Yu, Y. Wu, G. Li, *Nat. Photonics* **2009**, *3*, 649.
[14] H. J. Son, W. Wang, T. Xu, Y. Liang, Y. Wu, G. Li, L. Yu, *J. Am. Chem. Soc.* **2011**, *133*, 1885.
[15] a) S. Albrecht, S. Janietz, W. Schindler, J. Frisch, J. Kurpiers, J. Kniepert, S. Inal, P. Pingel, K. Fostiropoulos, N. Koch, D. Neher, *J. Am. Chem. Soc.* **2012**, *134*, 14932; b) L. Yang, J. R. Tumbleston, H. Zhou, H. Ade, W. You, *Energy Environ. Sci.* **2013**, *6*, 316.
[16] a) Y. Zhang, S.-C. Chien, K.-S. Chen, H.-L. Yip, Y. Sun, J. A. Davies, F.-C. Chen, A. K. Y. Jen, *Chem. Commun.* **2011**, *47*, 11026; b) Z. Fei, M. Shahid, N. Yaacobi-Gross, S. Rossbauer, H. Zhong, S. E. Watkins, T. D. Anthopoulos, M. Heeney, *Chem. Comm.* **2012**, *48*, 11130; c) Q. Peng, X. Liu, D. Su, G. Fu, J. Xu, L. Dai, *Adv. Mater.* **2011**, *23*, 4554; d) Y. Liang, D. Feng, Y. Wu, S.-T. Tsai, G. Li, C. Ray, L. Yu, *J. Am. Chem. Soc.* **2009**, *131*, 7792.
[17] B. A. Collins, J. Tumbleston, H. Ade, *J. Phys. Chem. Lett.* **2011**, *2*, 3135.
[18] a) R. Søndergaard, M. Manceau, M. Jørgensen, F. C. Krebs, *Adv. Energy Mater.* **2012**, *2*, 415; b) J. Alstrup, M. Jørgensen, A. J. Medford, F. C. Krebs, *ACS Appl. Mater.* **2010**, *2*, 2819.
[19] a) J. T. Rogers, K. Schmidt, M. F. Toney, E. J. Kramer, G. C. Bazan, *Adv. Mater.* **2011**, *23*, 2284; b) D. Chen, A. Nakahara, D. Wei, D. Nordlund, T. P. Russell, *Nano Lett.* **2010**, *11*, 561; c) T. Agostinelli, S. Lilliu, J. G. Labram, M. Campoy-Quiles, M. Hampton, E. Pires, J. Rawle, O. Bikondoa, D. D. C. Bradley, T. D. Anthopoulos, J. Nelson, J. E. Macdonald, *Adv. Funct. Mater.* **2011**, *21*, 1701.
[20] J. M. Szarko, J. Guo, Y. Liang, B. Lee, B. S. Rolczynski, J. Strzalka, T. Xu, S. Loser, T. J. Marks, L. Yu, *Adv. Mater.* **2010**, *22*, 5468.
[21] A. Hexemer, W. Bras, J. Glossinger, E. Schaible, E. Gann, R. Kirian, A. MacDowell, M. Church, B. Rude, H. Padmore, *J. Phys. Conf. Ser.* **2010**, *247*, 012007.
[22] J. Rivnay, R. Noriega, R. J. Kline, A. Salleo, M. F. Toney, *Phys. Rev. B* **2011**, *84*, 045203.
[23] a) S. Swaraj, C. Wang, H. Yang, B. Watts, J. Lüning, C. R. McNeill, H. Ade, *Nano Lett.* **2010**, *10*, 2863; b) H. Yan, B. A. Collins, E. Gann, C. Wang, H. Ade, C. R. McNeill, *ACS Nano* **2012**, *6*, 677.
[24] E. Gann, A. Young, B. A. Collins, H. Yan, J. Nasiatka, H. A. Padmore, H. Ade, A. Hexemer, C. Wang, *Rev. Sci. Instrum.* **2012**, *83*, 045110.
[25] B. A. Collins, Z. Li, J. R. Tumbleston, E. Gann, C. R. McNeill, H. Ade, *Adv. Energy Mater.* **2013**, *3*, 65.
[26] G. Porod, *Colloid Polym. Sci.* **1952**, *125*, 108.
[27] a) M. Campoy-Quiles, T. Ferenczi, T. Agostinelli, P. G. Etchegoin, Y. Kim, T. D. Anthopoulos, P. N. Stavrinou, D. D. C. Bradley, J. Nelson, *Nat. Mater.* **2008**, *7*, 158; b) D. S. Germack, C. K. Chan, R. J. Kline, D. A. Fischer, D. J. Gundlach, M. F. Toney, L. J. Richter, D. M. DeLongchamp, *Macromolecules* **2010**, *43*, 3828.
[28] J. A. Bartelt, Z. M. Beiley, E. T. Hoke, W. R. Mateker, J. D. Douglas, B. A. Collins, J. R. Tumbleston, K. R. Graham, A. Amassian, H. Ade, J. M. J. Fréchet, M. F. Toney, M. D. McGehee, *Adv. Energy Mater.* **2013**, DOI: 10.1002/aenm.201200637.
[29] B. P. Lyons, N. Clarke, C. Groves, *Energy Environ. Sci.* **2012**, *5*, 7657.
[30] a) B. A. Collins, E. Gann, L. Guignard, X. He, C. R. McNeill, H. Ade, *J. Phys. Chem. Lett.* **2010**, *1*, 3160; b) N. D. Treat, M. A. Brady, G. Smith, M. F. Toney, E. J. Kramer, C. J. Hawker, M. L. Chabinyc, *Adv. Energy Mater.* **2011**, *1*, 82; c) N. D. Treat, A. Varotto, C. J. Takacs, N. Batara, M. Al-Hashimi, M. J. Heeney, A. J. Heeger, F. Wudl, C. J. Hawker, M. L. Chabinyc, *J. Am. Chem. Soc.* **2012**, *134*, 15869.
[31] B. A. Collins, Z. Li, C. R. McNeill, H. Ade, *Macromolecules* **2011**, *44*, 9747.
[32] A. L. D. Kilcoyne, T. Tyliszczak, W. F. Steele, S. Fakra, P. Hitchcock, K. Franck, E. Anderson, B. Harteneck, E. G. Rightor, G. E. Mitchell, A. P. Hitchcock, L. Yang, T. Warwick, H. Ade, *J. Synchrotron Radiat.* **2003**, *10*, 125.
[33] B. A. Collins, H. Ade, *J. Electron. Spectrosc. Relat. Phenom.* **2012**, *185*, 119.
[34] H. W. Ro, B. Akgun, B. T. O'Connor, M. Hammond, R. J. Kline, C. R. Snyder, S. K. Satija, A. L. Ayzner, M. F. Toney, C. L. Soles, D. M. DeLongchamp, *Macromolecules* **2012**, *45*, 6587.
[35] C. G. Shuttle, R. Hamilton, B. C. O'Regan, J. Nelson, J. R. Durrant, *Proc. Natl. Acad. Sci. USA* **2010**, *107*, 16448.
[36] V. Mihailetchi, L. Koster, J. Hummelen, P. Blom, *Phys. Rev. Lett.* **2004**, *93*.
[37] a) R. A. Street, A. Krakaris, S. R. Cowan, *Adv. Funct. Mater.* **2012**; b) Z. M. Beiley, E. T. Hoke, R. Noriega, J. Dacuña, G. F. Burkhard, J. A. Bartelt, A. Salleo, M. F. Toney, M. D. McGehee, *Adv. Energy Mater.* **2011**, *1*, 954.
[38] P. K. Watkins, A. B. Walker, G. L. B. Verschoor, *Nano Lett.* **2005**, *5*, 1814.
[39] B. C. Schroeder, Z. Huang, R. S. Ashraf, J. Smith, P. D'Angelo, S. E. Watkins, T. D. Anthopoulos, J. R. Durrant, I. McCulloch, *Adv. Funct. Mater.* **2012**, *22*, 1663.
[40] B. A. Collins, J. E. Cochran, H. Yan, E. Gann, C. Hub, R. Fink, C. Wang, T. Schuettfort, C. R. McNeill, M. L. Chabinyc, H. Ade, *Nat. Mater.* **2012**, *11*, 536.